PERGAMON

International Journal of Solids and Structures 38 (2001) 1045–1062

INTERNATIONAL JOURNAL OF SOLIDS and STRUCTURES

www.elsevier.com/locate/ijsolstr

The influence of strain on confined electronic states in semiconductor quantum structures

H.T. Johnson [a,*], L.B. Freund [b]

[a] *Department of Aerospace and Mechanical Engineering, Boston University, Boston, MA 02215, USA*
[b] *Division of Engineering, Brown University, Providence, RI 02912, USA*

Received 16 April 1999

Abstract

A continuum finite element technique is adopted to study electronic properties of submicron electronic devices where function hinges on quantum mechanical effects. Of particular interest is the influence of mechanical strain on confined electronic states. The steady state Schrödinger equation, which governs the electronic behavior of such devices, is modified to include the potential induced by a strain field which is present as a consequence of the fabrication. The governing equation is cast in a variational form, and it is discretized on a standard finite element mesh which is more refined in regions where large quantum mechanical wave function gradients are expected. Multiple energy bands and three-dimensional structures can be considered, and effects including strain enhanced charge confinement and strain induced energy band mixing are studied. As examples, a Ge [5 0 1] faceted island, or quantum dot, on a Si substrate and a Ge v-groove quantum wire on a Si substrate are considered. The technique is used to determine size ranges in which these devices are expected to be most useful. The nonuniform mismatch strain field in the structures is found to affect the energies of experimentally accessible confined states and in some cases to enhance quantum mechanical confinement.

Keywords: Quantum dot; Nonuniform strain; Finite element; Schrödinger equation

1. Introduction

The study and characterization of semiconductor quantum devices has led to new problems and issues in continuum solid mechanics. Of particular interest is the class of devices that are composed of combinations of lattice mismatched materials. These material combinations, such as Si_xGe_{1-x}/Si and $In_xGa_{1-x}As/GaAs$, where x indicates the fractional content of alloying material, are selected primarily on the basis of their electronic properties and to some extent for convenience of processing, but high stresses induced by the constraint of heteroepitaxy often lead to defects or other undesirable mechanical effects. Even in devices free of misfit dislocations, the strain induced by lattice mismatch can strongly affect electronic properties.

* Corresponding author. Fax: +1-617-3535866.
E-mail address: hjohnson@bu.edu (H.T. Johnson).

0020-7683/01/$ - see front matter
PII: S0020-7683(00)00072-X

However, this effect has not been thoroughly studied, particularly in submicron sized structures in which quantum mechanics governs the device properties and in which strains are highest and most nonuniform.

In order to analyze strain effects in semiconductor quantum structures, it is necessary to adopt a model for electronic properties. Simple quantum mechanical models have long been available for describing the electronic properties of semiconductor devices based on the transport and confinement of single charge carriers. The study of quantum dots and quantum wires has renewed the interest in these models. The effects of uniform, coherent strain on electronic properties have also been well understood for many years. Recently, effects of mismatch induced nonuniform strain in semiconductor devices have been identified experimentally by Zaslavsky et al. (1995) and Akyüz et al. (1998), and there have been some attempts to model strain effects in quantum dots and quantum wires; see for example, Grundmann et al. (1995), Pryor (1998), Williamson et al. (1998), or Zunger (1998). Most work has been based on highly accurate but computationally intensive atomistic modeling.

While linear elastic strain in lattice mismatched semiconductor heterostructures is simple to characterize using standard structural analysis finite element packages, the use of the finite element method is very limited outside the field of solid mechanics. However, the simple quantum mechanical model governing the steady state behavior of single charge carriers in these semiconductor structures, based on the Schrödinger equation, is ideally suited for solution by means of the finite element method. Multiple coupled energy bands can be treated, as well as the effects of bimaterial interfaces and nonuniform strain effects.

Section 2 presents a well known, simple quantum mechanical model for electronic properties in semiconductor structures that has been modified to include the effects of strain. A finite element technique for solving the quantum mechanical problem is derived in the following section. Then, applications of the approach to the analysis of realistic Si_xGe_{1-x} quantum dots and quantum wires are presented and discussed. The effects of device size on quantum mechanical confinement and of nonuniform mismatch strain on confinement energies are considered.

2. Quantum mechanical model

The operation of semiconductor quantum devices is based on the confinement of individual electrons and holes in one spatial dimension (quantum wells), two spatial dimensions (quantum wires) or three spatial dimensions (quantum dots). Because quantum dots and wires are operated at extremely low temperatures and voltages, and because the length scales involved are very small, the effects of the scattering of electrons and holes can usually be neglected. Thus, it is possible to model the operation of these devices in terms of the ballistic transport of single charge carriers. As a starting point, the canonical quantum mechanics problem of the particle-in-a-box can be used to illustrate the confinement of charge carriers in quantum devices. The energy and wave function of the particle-in-a-box ground state for a finite potential well are shown schematically in Fig. 1.

In real quantum devices, the potential barriers forming the well are provided primarily by either free surfaces, which impose essentially infinite confinement, or by sharply layered compositional differences. In

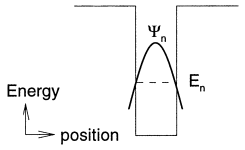

Fig. 1. A particle is confined to the potential well region and is characterized by energy E_n and wave function Ψ_n. The spatial probability density of the location of the particle is given by $|\Psi_n|^2$.

the SiGe system, for example, the valence bands of uniform bulk Si and Ge are shifted in energy by 0.46 eV. Thus, valence band charge carriers or holes in a Si layer of a device, experience a confining potential of 0.46 eV when surrounded by layers of Ge. This is a composition-based potential difference. Additional sources of potential in real heterostructures include applied voltage and elastic strain; it is the latter which is the primary focus of the work here. From deformation potential theory, the strain due to lattice mismatch, typically as large as several percent in magnitude, can be expected to induce potentials as large as 0.1 eV. Such a potential difference is significant compared to the composition based potential differences.

By adopting this continuum view of confinement in semiconductor quantum devices, the spectrum of confined states available to individual electrons or holes can be characterized by the steady state Schrödinger equation, given by

$$H^{\alpha\beta}(\vec{r})\Psi^{\beta}(\vec{r}) + V^{\alpha\beta}(\vec{r})\Psi^{\beta}(\vec{r}) = E\Psi^{\alpha}(\vec{r}), \tag{1}$$

where $H^{\alpha\beta}$ is the Hamiltonian function coupling the energy of a charge carrier between energy bands α and β, Ψ^{β} is the quantum mechanical wave function associated with energy band β, $V^{\alpha\beta}$ is an effective potential field coupling energy bands α and β, and E is the energy of a particular quantum mechanical state. Repeated Greek indices imply a summation over the energy band degrees of freedom, and $\vec{r}$ is the position vector throughout the solid. Analysis of confinement in a device is thus reduced to the study of an eigenvalue problem, where the unknown wave function Ψ^{α} is the eigenvector and the corresponding energy E is the eigenvalue. The solution of the problem depends on boundary conditions; free surfaces impose the physical requirement that $\Psi^{\alpha} = 0$ for all α. Conditions on boundaries that are remote from regions of interest in the device do not significantly affect energies or wave functions in regions of interest that are solutions to Eq. (1).

In order to proceed with the formulation of the boundary value problem, a quantum mechanical basis spanning the energy bands α and β must be chosen. In the case of the common material combination Si_xGe_{1-x}, which will be considered here, an appropriate quantum mechanical basis includes the highest energy valence subbands. This basis consists of the two degenerate *heavy hole* subbands and the two degenerate *light hole* subbands, in reference to the relative masses of the charge carriers when treated as classical particles. This choice of basis is sufficient because confinement in this material system occurs primarily in the valence band, and coupling between the highest energy valence subbands and other subbands in the material is very weak due to the large energy separation. The choice of the quantum mechanical basis, then, determines the tensor form of the Hamiltonian $H^{\alpha\beta}(\vec{r})$ and the potential field $V^{\alpha\beta}(\vec{r})$.

2.1. Hamiltonian function

The behavior of a charge carrier in various energy subbands in the presence of the periodic crystalline potential field is described by the Hamiltonian function. The well known $\boldsymbol{k}\cdot\boldsymbol{p}$ Hamiltonian of Kohn and Luttinger uses perturbation theory to describe semiconductor band structure away from wavevector $k = 0$ (Singh, 1993). This Hamiltonian can be used to model the medium in a Si_xGe_{1-x} structure using a four valence subband basis. The form of the $\boldsymbol{k}\cdot\boldsymbol{p}$ Hamiltonian is given by

$$H^{\alpha\beta}_{k\cdot p}(\vec{r}) = -\frac{\hbar^2}{2m_0}L^{\alpha\beta}_{ij}(\vec{r})\nabla^2_{ij}, \tag{2}$$

where $\hbar$ is Planck's constant, m_0 is the free electron mass, and the repeated indices indicate a summation over spatial coordinates. For α and β ranging over the four valence subbands referred to as h^+, h^-, l^+, and l^-, the matrices $L^{\alpha\beta}_{ij}(\vec{r})$ are given by

$$L^{h^+h^+}_{ij}(\vec{r}) = L^{h^-h^-}_{ij}(\vec{r}) = \begin{bmatrix} (\gamma_1+\gamma_2) & 0 & 0 \\ 0 & (\gamma_1+\gamma_2) & 0 \\ 0 & 0 & (\gamma_1-2\gamma_2) \end{bmatrix},$$

$$L_{ij}^{l^+l^+}(\vec{r}) = L_{ij}^{l^-l^-}(\vec{r}) = \begin{bmatrix} (\gamma_1-\gamma_2) & 0 & 0 \\ 0 & (\gamma_1-\gamma_2) & 0 \\ 0 & 0 & (\gamma_1+2\gamma_2) \end{bmatrix},$$

$$L_{ij}^{h^+l^+}(\vec{r}) = L_{ij}^{l^+h^{+*}}(\vec{r}) = -L_{ij}^{h^-l^{-*}}(\vec{r}) = -L_{ij}^{l^-h^-}(\vec{r}) = \begin{bmatrix} 0 & 0 & -i\sqrt{3}\gamma_3 \\ 0 & 0 & -\sqrt{3}\gamma_3 \\ -i\sqrt{3}\gamma_3 & -\sqrt{3}\gamma_3 & 0 \end{bmatrix},$$

$$L_{ij}^{h^+l^-}(\vec{r}) = L_{ij}^{h^-l^{+*}}(\vec{r}) = L_{ij}^{l^+h^-}(\vec{r}) = L_{ij}^{l^-h^{+*}}(\vec{r}) = \begin{bmatrix} \sqrt{3}\gamma_2 & -i\sqrt{3}\gamma_3 & 0 \\ -i\sqrt{3}\gamma_3 & -\sqrt{3}\gamma_2 & 0 \\ 0 & 0 & 0 \end{bmatrix},$$

$$L_{ij}^{h^+h^-}(\vec{r}) = L_{ij}^{h^-h^+}(\vec{r}) = L_{ij}^{l^+l^-}(\vec{r}) = L_{ij}^{l^-l^+}(\vec{r}) = \begin{bmatrix} 0 & 0 & 0 \\ 0 & 0 & 0 \\ 0 & 0 & 0 \end{bmatrix}, \tag{3}$$

where γ_1, γ_2, and γ_3 are the Luttinger–Kohn parameters. These material parameters for Si and Ge, as well as additional details on the form of $L_{ij}^{\alpha\beta}(\vec{r})$, are given in Appendix A.

2.2. Spatially varying potential field

The nonuniform potential field $V^{\alpha\beta}(\vec{r})$ includes all energetic effects on the charge carrier due to sources other than the background periodic crystalline potential. In the analysis presented here, the effects to be considered include the relative offset of the valence band in adjacent layers of the heterostructure, and the effect of the elastic strain field. The potential field can be written as the sum of these two contributions, so that

$$V^{\alpha\beta}(\vec{r}) = V_{\text{band}}^{\alpha\beta}(\vec{r}) + V_{\text{strain}}^{\alpha\beta}(\vec{r}). \tag{4}$$

Other effects can also be considered including, for example, the effect of a piezoelectric potential induced by strain. This effect is not expected to be significant here, nor is the effect of the correction of the total potential $V^{\alpha\beta}(\vec{r})$ for self-consistency.

The band structure contribution $V_{\text{band}}^{\alpha\beta}(\vec{r})$ to the total potential is due to the energy misalignment of the valence band maxima in adjacent layers of material, which is proportional to the Si concentration in a Si_xGe_{1-x} structure. In this material system, the conduction band minima are known to coincide in energy, so that the valence bands are misaligned by the entire bandgap offset energy, $\Delta E_{\text{bg}} = E_{\text{bg}}^{\text{Si}} - E_{\text{bg}}^{\text{Ge}}$. Thus, for a valence band model in the Si_xGe_{1-x} system, the value of this contribution to the potential is given by

$$\begin{aligned} V_{\text{band}}^{\alpha\beta}(\vec{r}) &= x(\vec{r})\Delta E_{\text{bg}}, \quad \alpha = \beta, \\ V_{\text{band}}^{\alpha\beta}(\vec{r}) &= 0, \quad \alpha \neq \beta, \end{aligned} \tag{5}$$

where $x(\vec{r})$ is the Si concentration as a function of position.

Elastic strain in the structure induces a potential that shifts and couples the energy bands in the crystal. Based on deformation potential theory, the calculated strain tensor ϵ_{ij} can be used to generate a potential by means of the operation

$$V_{\text{strain}}^{\alpha\beta}(\vec{r}) = D_{ij}^{\alpha\beta}(\vec{r})\epsilon_{ij}(\vec{r}) \tag{6}$$

in which $D_{ij}^{\alpha\beta}$, for $\alpha = \beta$, imposes a strain induced shift in the potential $V_{\text{strain}}^{\alpha\beta}(\vec{r})$ and, for $\alpha \neq \beta$, imposes strain induced band coupling. The form of $D_{ij}^{\alpha\beta}(\vec{r})$ is similar to the form of $L_{ij}^{\alpha\beta}(\vec{r})$ given in Eq.(3). The

components of $D_{ij}^{\alpha\beta}(\vec{r})$ can be obtained from the components of $L_{ij}^{\alpha\beta}(\vec{r})$ by means of the variable substitutions: $(\hbar^2/2m_0)\gamma_1 \leftrightarrow a$, $(\hbar^2/m_0)\gamma_2 \leftrightarrow b$, $(\sqrt{3}\hbar^2/m_0)\gamma_3 \leftrightarrow d$, where a, b, and d are material constants. These constants have been compiled from experimental measurements and can also be predicted on the basis of first principles calculations. Values of the material constants used to characterize Si and Ge, and some additional details about the form of the deformation potential tensor $D_{ij}^{\alpha\beta}(\vec{r})$ and the Hamiltonian function $H_{k\cdot p}^{\alpha\beta}(\vec{r})$, are given in Appendix A.

3. Finite element formulation

The nonuniform steady state Schrödinger equation (1), which governs the behavior of individual charge carriers in strained devices, is in the form of the Helmholtz equation. Like the linear elastic wave equation for harmonic wave motion, it can be cast into a variational framework which serves as the basis for a standard boundary value problem using the finite element method.

3.1. Variational formulation of the governing equation

The form of the Schrödinger equation to be solved is

$$-\frac{\hbar^2}{2m_0}L^{\alpha\beta}(\vec{r})\nabla^2\Psi^{\beta}(\vec{r}) + V^{\alpha\beta}(\vec{r})\Psi^{\beta}(\vec{r}) = E\Psi^{\alpha}(\vec{r}). \tag{7}$$

The weak form of the equation is obtained by forming the inner product of each term in the equation with the wave function vector field $\Psi^{\alpha}(\vec{r})$ and integrating over the volume of the body. The first term is integrated by parts, and the functional corresponding to the weak form is given by

$$\Pi(\Psi^{\alpha}) = -\frac{\hbar^2}{2m_0}\int_R \nabla\Psi^{\alpha}L^{\alpha\beta}\nabla\Psi^{\beta}\,\mathrm{d}R + \int_R \Psi^{\alpha}V^{\alpha\beta}\Psi^{\beta}\,\mathrm{d}R - E\int_R \Psi^{\alpha}\Psi^{\beta}\,\mathrm{d}R. \tag{8}$$

Eq. (7) is the Euler equation which results from the requirement that Eq. (8) must be stationary under variations in Ψ^{α}. The body is then discretized into nodes and elements, so that spatially varying fields can be expressed in terms of nodal values and element shape functions $N(\vec{r})$. These fields are written as,

$$\Psi^{\alpha} = \sum_{A=1}^{\text{all nodes}} \Psi_A^{\alpha}N_A(\vec{r}), \qquad \nabla\Psi^{\alpha} = \sum_{B=1}^{\text{all nodes}} \Psi_B^{\alpha}\nabla N_B(\vec{r}), \qquad V^{\alpha\beta} = \sum_{C=1}^{\text{all nodes}} V_C^{\alpha\beta}N_C(\vec{r}). \tag{9}$$

The functional $\Pi(\Psi^{\alpha})$ can then be approximated by the discrete form

$$\Pi(\Psi_A^{\alpha}) = \frac{-\hbar^2}{2m_0}\int_R \Psi_A^{\alpha}\nabla N_A L^{\alpha\beta}\Psi_B^{\beta}\nabla N_B\,\mathrm{d}R + \int_R \Psi_A^{\alpha}N_A V_C^{\alpha\beta}N_C\Psi_B^{\beta}N_B\,\mathrm{d}R - E\int_R \Psi_A^{\alpha}\Psi_B^{\beta}N_A N_B\,\mathrm{d}R, \tag{10}$$

where repeated capital Roman subscripts indicate a summation over all nodes. The quadratic function is then rendered stationary with respect to the nodal values of the wave function Ψ_B^{β} according to the condition

$$\frac{\mathrm{d}\Pi(\Psi_A^{\alpha})}{\mathrm{d}\Psi_B^{\beta}} = 0. \tag{11}$$

The term containing the Hamiltonian represents kinetic energy while the term containing the nonuniform potential represents potential energy. This condition on the wave function Ψ_A^{α} leads to the equation

$$\Psi_A^\alpha \left[-\frac{\hbar^2}{2m_0} \int_R \nabla N_A L^{\alpha\beta} \nabla N_B \, \mathrm{d}R + \int_R N_A V_C^{\alpha\beta} N_C N_B \, \mathrm{d}R - E \int_R N_A N_B \, \mathrm{d}R \right] = 0. \tag{12}$$

The integrals over the region R can be replaced with integrals over individual element volumes (Ω^e) and a summation over all elements in order to obtain the finite element form of the governing equation, which is written as

$$\sum^{\text{elems}} \left[\int_{\Omega^e} \left(\frac{-\hbar^2}{2m_0} \nabla N_A L^{\alpha\beta} \nabla N_B + N_A N_B V_C^{\alpha\beta} N_C \right) \mathrm{d}\Omega \right] \Psi_B^\beta = E \sum^{\text{elems}} \left[\int_{\Omega^e} N_A N_B \, \mathrm{d}\Omega \right] \Psi_B^\alpha. \tag{13}$$

The integration over each element volume (Ω^e) is done by Gaussian quadrature of a degree which is exact for the shape functions selected. In the terminology of structural mechanics, the contribution of a single element to the left-hand side of the equation is given by the element "stiffness" matrix; contributions to the right side of the equation are due to element "mass" matrices. For a problem with m spatial dimensions and an n subband quantum mechanical basis, the element stiffness and mass matrices have size $(m^2 n \times m^2 n)$. The element matrices are defined by,

$$\begin{aligned} k_{\alpha\beta}^e &= \sum_{l=1}^{\text{int.pts.}} \left(\frac{-\hbar^2}{2m_0} \nabla N_A L^{\alpha\beta} \nabla N_B + N_A V_C^{\alpha\beta} N_C N_B \right)_l, \\ m^e &= \sum_{l=1}^{\text{int.pts.}} (N_A N_B)_l. \end{aligned} \tag{14}$$

The final finite element matrix form of the Schrödinger equation is constructed by assembling the element stiffness and mass matrices into global stiffness and mass matrices K_{ij} and M_{ij}, where i and j range over all $n\alpha$ global degrees of freedom, where n is the number of nodes and α is the number of energy subbands in the quantum mechanical basis. The finite element formulation of the governing equation then takes the form

$$K_{ij} \Psi_j = E M_{ij} \Psi_j, \tag{15}$$

which, as a generalized eigenvalue problem, is ideally suited for computation. The unknown wave function Ψ_j is the eigenvector and the unknown energy E is the eigenvalue.

3.2. Spectrum of energies and wave functions

The finite element solution of the Schrödinger equation consists of a spectrum of energies and corresponding wave functions. There are $n\alpha$ solutions, equal in number to the number of global degrees of freedom in the system. For each solution with energy E, the corresponding wave function Ψ^α has components in each subband α. Some states consist predominantly of a single wave function component, while other states have mixed wave function components.

In general, the lowest energy states or ground states, which are of the most practical interest in assessing device properties of quantum semiconductor structures, will be determined with the greatest numerical accuracy. Due to the low temperatures and operating voltages used in experiments, only these lower energy confined states are needed for the analysis of real semiconductor quantum structures. Some accuracy is lost in the numerical calculation of the excited states.

Furthermore, in studying devices that are based on quantum mechanical confinement, it is only necessary to consider a subset of the $n\alpha$ solutions of the governing equation. Many eigenstates, in general, represent steady state solutions in which the wave function is not confined to a region of interest in the structure. At low energies, some of these nonlocalized states represent spurious numerical results due, for

example, to the choice of remote boundary conditions but which do not affect regions of interest in the structure. Thus, it is necessary to examine only low energy states which are confined to the region of interest in the structure.

4. Examples

Two SiGe quantum structures are analyzed as examples of the finite element technique. Both devices are of particular interest because of the effects of strain, which is induced during the heteroepitaxial growth process. The mismatch strain has consequences for the resulting morphology of the surface, and as is shown here, for the electronic properties of the resulting devices. The continuum finite element approach is also useful for evaluating the strong size effects on confinement energies in the structures.

The electronic properties analysis for the quantum devices consists primarily of the determination of confinement energies. Due to the experimentally understood nature of energy band alignment in SiGe heterostructures, the calculations in both examples are for valence band properties. The convention is adopted whereby zero energy occurs at the common Si and Ge conduction band minimum, with energy increasing towards the valence band, as illustrated in Fig. 2. The Ge valence band edge occurs at +0.66 eV and the Si valence band edge occurs at +1.12 eV. A confinement occurs in the energy range between 0.66 V and 1.12 eV, with more (less) strongly confined states occurring at lower (higher) energies.

4.1. Faceted island quantum dot

The island growth mode in strained heteroepitaxy of thin film systems has been the focus of intense research lately because of possible quantum dot applications. The growth of islands on a substrate, also known as the Stranski–Krastanow growth mode, has been identified and understood in the Si_xGe_{1-x} system for at least the past decade (Eaglesham and Cerullo, 1990). It has been suggested more recently that this

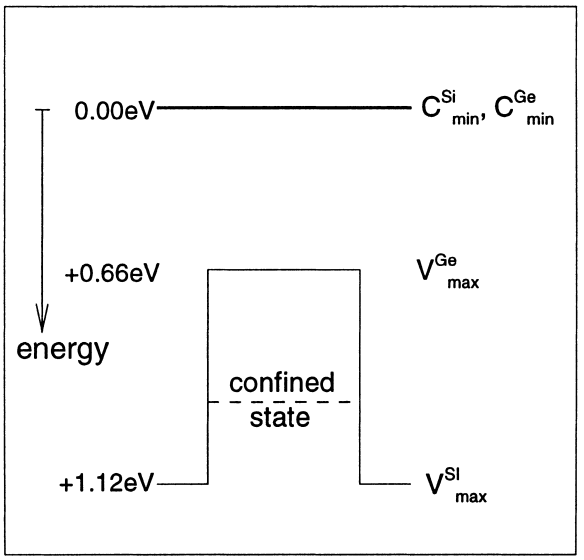

Fig. 2. Schematic of the energy and sign convention adopted here. Confined states occur in the quantum well region and have energies between 0.66 eV and 1.12 eV.

type of surface morphology, originally thought to be defective, could be applied for the fabrication of quantum dot arrays (Leonard et al., 1993).

From the work of Floro et al. (1997), it is known that the pyramid shaped Ge islands self assemble under certain conditions during heteroepitaxy on Si substrates. The island faces are formed by distinctive [5 0 1] crystallographic planes. The geometry, size and arrangement of the arrays of these islands are sensitive to experimental conditions. The island sizes range in reported base width from less than 10 nm to over 100 nm; this size scale is associated with potential quantum dot applications. The potential of these structures to be used as quantum dots, as well as the effects of strain on the electronic properties of the structures, can be assessed directly using the finite element technique presented here.

A three dimensional finite element mesh is first set up for an individual isolated island. The same mesh can be used in this case for calculating both the linear elastic strain field and the spectrum of quantum mechanical confined states. A portion of the mesh for a single [5 0 1] faceted Ge quantum dot is shown in Fig. 3.

The lateral size of the substrate in the full finite element mesh is approximately $(3w \times 3w)$, with a substrate thickness of approximately w, where w is the island width. These dimensions are assumed to approximate the case of an isolated island. The height of the island, fixed by the geometry of the [5 0 1] surfaces, is $w/10$. With the substrate size large, compared to the island size, both linear elastic fields and quantum mechanical wave functions are relatively insensitive to remote boundary conditions.

The linear elasticity boundary value problem, arising from the mismatch in lattice parameters between the island and substrate materials, is solved using a standard structural mechanics finite element package (ABAQUS, 1997). The lattice mismatch is affected by applying a uniform expansion in the island material equal to the lattice parameter mismatch, by requiring displacement compatibility across the island/substrate interface, and then by allowing the system to relax to a minimum energy configuration. This approach is comparable to the shrink-fit or Eshelby inclusion approach, whereby a stress free transformation strain is applied to a region by means of artificial tractions. The strain relaxation which occurs as the artificial tractions are removed must be accommodated by the surrounding material (Eshelby, 1957). All outer boundaries of the mesh are considered to be traction free surfaces in this case.

A resulting lateral extensional strain component in the island is shown in Fig. 4. Because the material is assumed to be isotropic, the strain fields are symmetric with respect to the lateral directions. However, the strain field is nonuniform as a result of the relaxation of the island free surfaces. The region near the base of the island is strained nearly to the level of the system mismatch of approximately four percent. The island apex, however, is almost strain free due to the proximity of the free surfaces.

The quantum mechanical calculation is then formulated to include the effects of the linear elastic strain fields. In this case, the quantum mechanical basis for the [5 0 1] Ge island is taken to be a single heavy hole valence subband. Because of the full three dimensional geometry of the structure, this reduced basis is

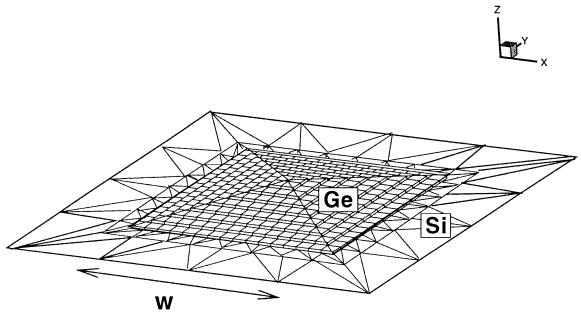

Fig. 3. Finite element mesh for the region near a [5 0 1] Ge island on a Si substrate. The island edges are outlined for clarity.

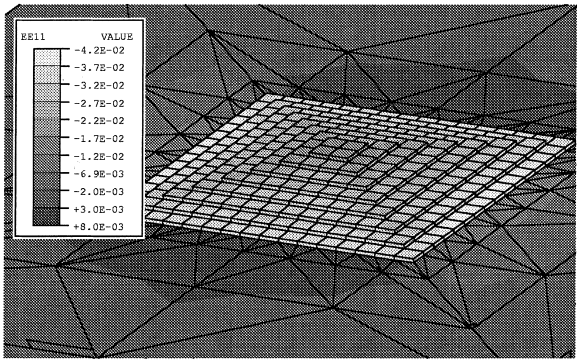

Fig. 4. Lateral extensional component of strain in a [5 0 1] Ge island. The substrate is nearly unstrained, the base of the island is highly compressively strained, and the strain at the apex of the island is mostly relaxed by the free surfaces.

chosen in order to limit the number of degrees of freedom which must be considered. This substantially reduces the cost of the computation but at some expense to the basic physical model. Strain induced band mixing, which may be physically significant in this case, is neglected as a result of this assumption. Due to the choice of the single subband basis, the potential field becomes scalar valued. A cross-sectional view of the strain effects on the potential field is shown in Fig. 5. While the primary source of the relative confining potential in the Ge island is the offset in the valence band maxima between Ge and Si of 0.46 eV, mismatch strain also has an important effect. Strain locally increases the potential near the base of the island, which is highly strained, and reduces the potential near the apex and edges of the island, where the strain is mostly relaxed. It is worth noting that the potential in the substrate is also affected by the strain field, because the wave function for a given state may not be completely confined to the film.

The nonhomogeneous Schrödinger equation is then solved using the finite element method, formulated to include three spatial dimensions and one quantum mechanical dimension which, in this case, is taken to be the heavy hole valence subband. The components of the effective mass tensor for this energy band basis are given in Appendix A. The solution yields a spectrum of eigenstates for the single subband. Confined

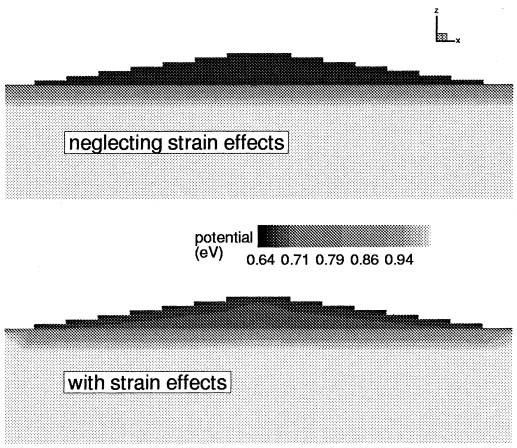

Fig. 5. Potential field in a [5 0 1] Ge island on a Si substrate. The primary potential difference is due to the relative valence band offset in Ge with respect to Si; mismatch strain also affects the potential.

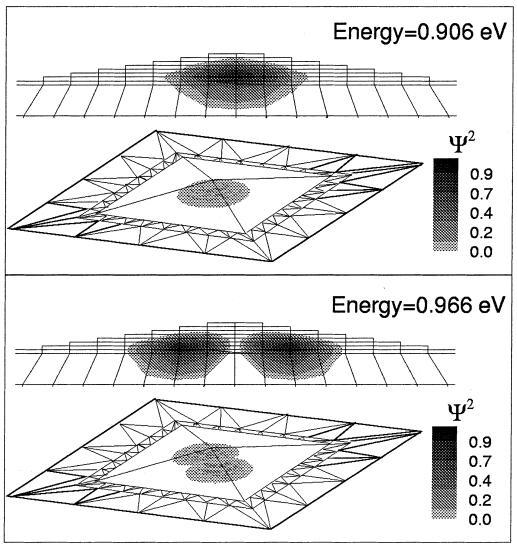

Fig. 6. Probability density fields for lowest two heavy hole states in a 30 nm island. The states are almost entirely confined to the island region, and are separated in energy by 60 meV.

states, with energies falling between the valence band maximum energy in bulk Ge and the valence band maximum energy in bulk Si, are observed in some islands.

Probability density profiles, given by the square of the wave function fields, for the two lowest energy states in an island with base width of 30 nm, are shown in Fig. 6. The linear elastic strain fields, and thus the scalar potential fields, are independent of island width for fixed island shape, but confinement is nonetheless strongly dependent on island width. For example, no confined states are observed in islands of width less than 10 nm, which is within the range of experimentally observed island sizes. For islands of width greater than approximately 50 nm, which is also within the range of experimentally observed sizes, there are hundreds of confined states, with the largest energy separation being less than 10 meV. Smaller energy separations between confined states are generally less desirable in practical applications due to the difficulty in measuring small energy differences. The effects of island size on the spectra of confined states are summarized in Fig. 7.

Finally, the addition of strain effects in the finite element model of the Schrödinger equation is shown to significantly affect confinement energies. Strain effects lead to higher confinement energies, characteristic of smaller islands in an unstrained case, but smaller separation energies, characteristic of larger islands in an unstrained case. Fig. 8 shows the direct effect of strain on the energies of confined states in a 20 nm island. The reduction of the energy of separation between states has potentially significant experimental implications, particularly in some optical applications, for example, where precise control over confinement energies is needed to optimize device output.

4.2. V-groove quantum wire

A number of experimental and theoretical studies have been reported recently on semiconductor structures referred to as quantum wires (Brinkmann et al., 1996; Yang et al., 1997; Faux et al., 1997). In the literature, long narrow structures with lateral dimensions of less than a micron are often given this label. There are many proposed techniques for fabricating the structures, including the intriguing possibility of self-assembly. Various other techniques rely on lithography.

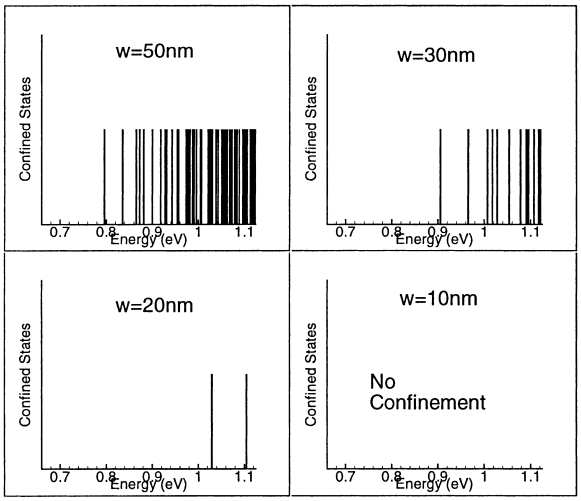

Fig. 7. Confined states in Ge islands as a function of island width. Many states are available in islands of 50 nm or larger, but the energy spacing may be experimentally insignificant. In islands of 10 nm or less, no confinement is observed. In 20 nm islands, confined states are seen at only two energies, separated by 75 meV, with the ground state at 1030 meV from the bulk Ge valence band energy.

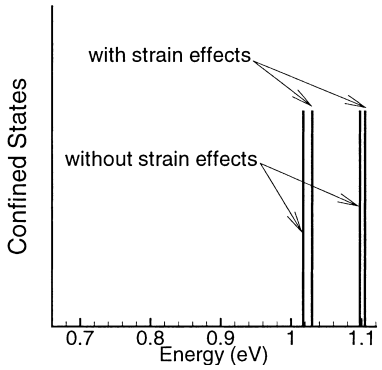

Fig. 8. Effect of strain on confinement energies in a 20 nm island. Energies of both confined states are increased by strain, and the energy of separation is reduced by 10 meV.

One promising method for producing quantum wire structures uses a chemical etch technique to pattern v-shaped grooves into the surface of a semiconductor substrate. Epitaxial film material is then deposited into the grooves. Due to the energy band misalignment effect between the film and substrate materials, and very small dimensions of the structure, quantum confinement in the lateral direction is expected, while charge is free to move in the longitudinal direction. A cross sectional schematic view of two v-groove quantum wires is shown in Fig. 9. In addition to energy band misalignment, in some cases the film and substrate materials have mismatched lattice parameters, as in the case of Ge wires in a Si substrate. The constraint across the interface results in nonuniform strain which has an additional effect on the quantum mechanical confinement.

The case of a strained Ge quantum wire in a Si substrate is considered here. As was done for the case of an island, a single finite element mesh is used to model the cross section of an isolated v-groove wire, for both the linear elasticity and quantum mechanics calculations. The configuration consists of a large Si

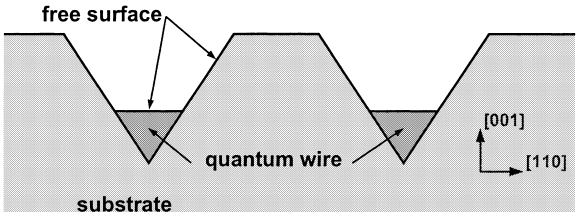

Fig. 9. The two parallel v-groove quantum wires are fabricated by epitaxially depositing film material into grooves etched in the substrate.

substrate region, extending several times the wire width in all directions, and a Ge wedge shaped film region, with side faces along [1 1 0] planes and the top surface along a [1 0 0] plane.

Both the linear elasticity problem and the quantum mechanical problem can be modeled completely using this two-dimensional representation, due to the fact that the wire is much longer than it is wide. This feature allows the elasticity problem to be reduced to the case of plane strain, and the quantum mechanical problem to be reduced to the case of a free particle, with the appropriate effective mass, in the direction normal to the cross section.

The linear elasticity problem of solving for the mismatch induced nonuniform strain field is accomplished using the general purpose finite element code ABAQUS. A uniform dilatation, in the amount of the lattice mismatch, is imposed on the Ge wire material, and then displacement compatibility is imposed across the Ge/Si interface. The system reaches an equilibrium, and due to the free surface relaxation effect, the strain field is nonuniform. The lateral extensional component of strain in the structure is shown in Fig. 10.

Because the problem can be handled using a two dimensional spatial basis, it is then possible to manage the additional computational cost of adopting a four-subband quantum mechanical basis. The basis used here, as is common for the Ge/Si material system, includes the two degenerate heavy hole valence subbands and the two degenerate light hole valence subbands. With this basis, there are four components of the potential field that must be calculated. The potential field components are shown in Fig. 11. For fixed geometry, these potential field components are independent of the wire size due to the use of linear elasticity for the solution of the strain field.

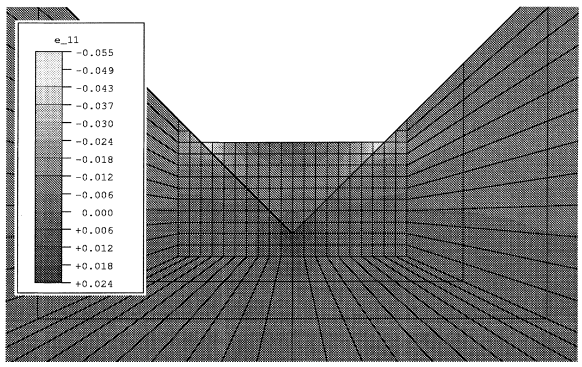

Fig. 10. The four percent mismatch between the film and substrate material results in a nonuniform strain field in and near the v-groove quantum wire. The lateral extensional strain is highly compressive near the top corners of the wire, while the strain is tensile in the bottom of the groove.

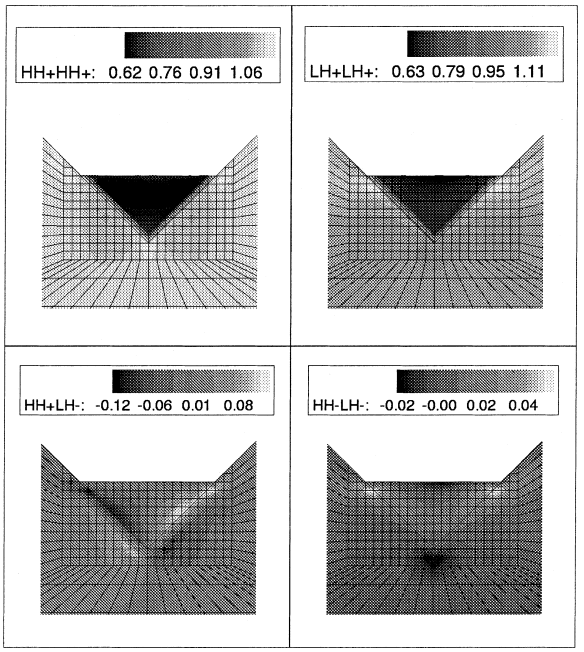

Fig. 11. The two upper plots are components of the potential that directly affect states in the heavy hole and light hole subbands, and are due to the superposition of band offset contributions and strain contributions. The lower plots are potentials that couple the subbands, and are due only to strain. Energies are in units of eV.

As in the analysis of the quantum dot, the solution of the Schrödinger equation for the v-groove quantum wire consists of a spectrum of energies and associated wave functions. Due to the choice of the four subband basis in this case, however, the wave function is vector valued, with components in each of the subbands. The $\boldsymbol{k} \cdot \boldsymbol{p}$ Hamiltonian leads to eigenstates with components in both the heavy hole and light hole subbands. Strain lifts the degeneracy of the subbands, and it also energetically separates heavy hole states from light hole states. Representative wave functions in the four subbands for a low energy confined state in a wire of width $w = 10$ nm are shown in Fig. 12. The energy state has major components in heavy hole and light hole subbands. However, in the analyses presented here, because of the relatively coarse discretization of the wire region, limited information can be obtained about the spatial form of the wave functions for excited states.

Some conclusions can be drawn about confinement energies in the wires. First, it is straightforward to examine the effect of wire width on the spectrum of confined states. The smallest wires considered, with width $w = 10$ nm, have reasonably large energy separation between confined states, on the order of 100 meV. Larger structures have much more closely spaced confinement energies which would be indistinguishable experimentally. The spectra of confined states for two wires, with width of 10 and 25 nm, are shown in Fig. 13. The difference in size between the two wires has a significant effect on confinement energies. Confinement energies for the lowest states in the wire of width 25 nm are roughly 10 meV; higher energy confined states are essentially continuous. The energies separating confined states in a wire as large as 100 nm would be practically negligible.

Strain effects on confinement energies are relatively large in the v-groove wires. By removing the strain induced contribution to the nonuniform potential, it can be shown that the presence of the strain tends to reduce the confinement energies of most states for this structure. Fig. 14 shows confinement spectra for the

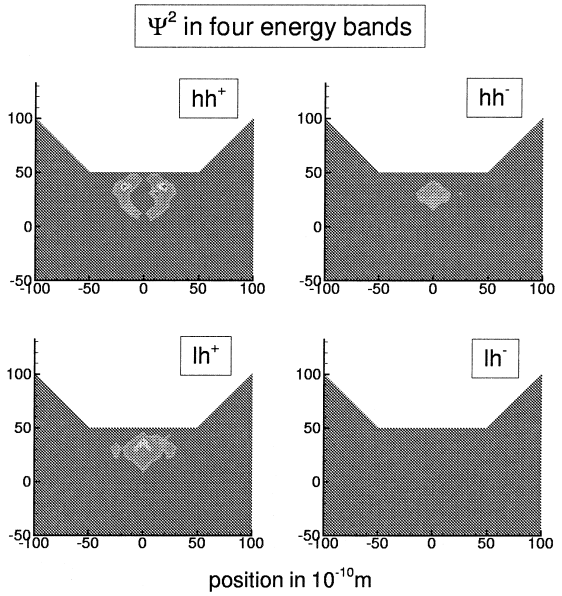

Fig. 12. A confined state in a v-groove quantum wire of width $w = 10$ nm has major wave function components in two of the four heavy hole and light hole subbands.

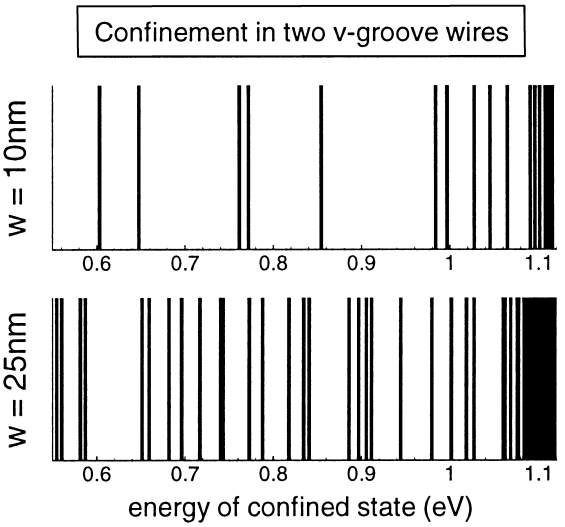

Fig. 13. Confinement energies in the $w = 10$ nm v-groove quantum wire are on the order of 100 meV. Confined states are much more closely spaced in the $w = 25$ nm wire; higher energy confined states practically appear continuous.

wire of width $w = 10$ nm both with and without considering the strain effects. The strain field affects the higher energy states more strongly, and near the upper limit of the energy range, additional states are confined by the strain.

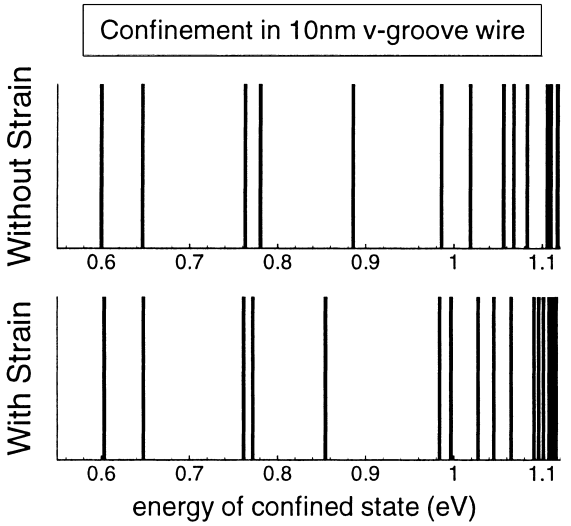

Fig. 14. The addition of the strain contribution to the potential has a stronger effect on higher energy confined states in the $w = 10$ nm v-groove quantum wire. Additional states are confined simply due to the strain field.

5. Conclusions

The analysis of electronic properties of strained semiconductor structures is reduced here to the solution of a linear boundary value problem, for which an approximate solution is readily found by means of the finite element method. The finite element approach is based on a variational formulation of the time independent Schrödinger equation. While the quantum mechanical model neglects some features of the physical problem, the ease of use of the finite element method for solving the governing equations makes the method an attractive way of probing basic energetics in structures that are based on quantum confinement. Due to the concept of the linear superposition of the sources of effective potential on the single charge carrier, it is possible in the analysis to isolate the effects of strain, which is important in understanding the large class of devices consisting of lattice mismatched heterostructure materials.

The two specific structures considered here vary in both the number of the spatial dimensions and in the size of the quantum mechanical basis. The [5 0 1] island quantum dot analysis requires a full three dimensional analysis for both the elasticity problem (although some symmetry can be exploited) and the quantum mechanics problem. Due to the large number of nodal degrees of freedom required, it is more practical then to consider only a single subband quantum mechanical model. In the case of the v-groove quantum wire, where both the linear elasticity problem and the quantum mechanics problem were essentially two dimensional, it is not difficult to consider a four subband basis, which allows for the study of strain induced band mixing. These problems are computationally efficient; all calculations reported here were performed on a DEC Alpha workstation.

Spectra of confined electronic states are calculated for both structures. Strain effects can be isolated from the effects of relative bandgap offsets in the material, and it is shown that strain changes the energy separation of confined states that may be experimentally accessible. Furthermore, studies of the effects of device size on confinement can be carried out simply by scaling nodal coordinates in the quantum mechanics finite element analysis. It is shown that for both the [5 0 1] pyramidal quantum dot and the v-groove quantum wire there is a narrow range of sizes in which the confined states are likely to be useful in real devices. In the pyramidal quantum dot, for example, it is found that the base width of the SiGe islands

should be in the range of 10–50 nm in order for confined heavy hole valence band states to be most useful. In the v-groove quantum wires, which would be expected to be most useful with a width of approximately 10 nm, strain is found to induce band mixing, to more strongly affect the energies of the more excited confined states, and to actually lead to the presence of additional confined states.

For the structures considered here, the scaling of the features does not affect the linear elastic strain fields. Thus, the inferred useful size ranges for the devices are based purely on quantum mechanical effects. However, in structures with sizes that are characterized by multiple physical length scales, the scaling of structural features can also affect strain fields (Johnson et al., 1998). For example, pyramidal islands of varying base widths but fixed volume, without the restriction of [5 0 1] faceted sides, would have size dependent strain fields. This additional effect on confinement energies in devices could also be probed using the approach presented here.

The analysis of strain effects in semiconductor quantum structures is achieved here using a computationally efficient and practical continuum finite element approach. Similar modeling with better quantum mechanical accuracy is possible using fully atomistic approaches. However, the wide range of structures and devices of all sizes that can be considered using this approach make the technique a useful tool. The realistic SiGe structures considered here exhibit strong coupling of strain and electronic properties; predictive modeling of this phenomenon is important in the design and interpretation of future experimental work.

Acknowledgements

The research support of the Office of Naval Research, Contract N00014-95-1-0239, and the MRSEC Program of the National Science Foundation, under Award DMR-9632524, at Brown University is gratefully acknowledged.

Appendix A

The strain induced potential $V_{\epsilon}^{\alpha\beta}(\vec{r})$ is given by

$$V_{\epsilon}^{\alpha\beta}(\vec{r}) = \begin{array}{c} \\ |\tfrac{3}{2},+\tfrac{3}{2}\rangle \\ |\tfrac{3}{2},-\tfrac{3}{2}\rangle \\ |\tfrac{3}{2},+\tfrac{1}{2}\rangle \\ |\tfrac{3}{2},-\tfrac{1}{2}\rangle \end{array} \begin{array}{c} \begin{array}{cccc} |\tfrac{3}{2},+\tfrac{3}{2}\rangle & |\tfrac{3}{2},-\tfrac{3}{2}\rangle & |\tfrac{3}{2},+\tfrac{1}{2}\rangle & |\tfrac{3}{2},-\tfrac{1}{2}\rangle \end{array} \\ \begin{pmatrix} D_{ij}^{11}(\vec{r})\epsilon_{ij}(\vec{r}) & D_{ij}^{12}(\vec{r})\epsilon_{ij}(\vec{r}) & D_{ij}^{13}(\vec{r})\epsilon_{ij}(\vec{r}) & D_{ij}^{14}(\vec{r})\epsilon_{ij}(\vec{r}) \\ D_{ij}^{21}(\vec{r})\epsilon_{ij}(\vec{r}) & D_{ij}^{22}(\vec{r})\epsilon_{ij}(\vec{r}) & D_{ij}^{23}(\vec{r})\epsilon_{ij}(\vec{r}) & D_{ij}^{24}(\vec{r})\epsilon_{ij}(\vec{r}) \\ D_{ij}^{31}(\vec{r})\epsilon_{ij}(\vec{r}) & D_{ij}^{32}(\vec{r})\epsilon_{ij}(\vec{r}) & D_{ij}^{33}(\vec{r})\epsilon_{ij}(\vec{r}) & D_{ij}^{34}(\vec{r})\epsilon_{ij}(\vec{r}) \\ D_{ij}^{41}(\vec{r})\epsilon_{ij}(\vec{r}) & D_{ij}^{42}(\vec{r})\epsilon_{ij}(\vec{r}) & D_{ij}^{43}(\vec{r})\epsilon_{ij}(\vec{r}) & D_{ij}^{44}(\vec{r})\epsilon_{ij}(\vec{r}) \end{pmatrix} \end{array}, \tag{A.1}$$

where each component $D_{ij}^{\alpha\beta}(\vec{r})$ of the matrix for fixed $\alpha\beta$ forms a scalar product with the strain tensor $\epsilon_{ij}(\vec{r})$ through summation over i and j. And similarly, the $\boldsymbol{k}\cdot\boldsymbol{p}$ Hamiltonian given by Luttinger and Kohn takes the form

$$H_{k\cdot p}^{\alpha\beta}(\vec{r}) = \begin{array}{c} \\ |\tfrac{3}{2},+\tfrac{3}{2}\rangle \\ |\tfrac{3}{2},-\tfrac{3}{2}\rangle \\ |\tfrac{3}{2},+\tfrac{1}{2}\rangle \\ |\tfrac{3}{2},-\tfrac{1}{2}\rangle \end{array} \begin{array}{c} \begin{array}{cccc} |\tfrac{3}{2},+\tfrac{3}{2}\rangle & |\tfrac{3}{2},-\tfrac{3}{2}\rangle & |\tfrac{3}{2},+\tfrac{1}{2}\rangle & |\tfrac{3}{2},-\tfrac{1}{2}\rangle \end{array} \\ \begin{pmatrix} L_{ij}^{11}(\vec{r})\nabla_{ij}^2 & L_{ij}^{12}(\vec{r})\nabla_{ij}^2 & L_{ij}^{13}(\vec{r})\nabla_{ij}^2 & L_{ij}^{14}(\vec{r})\nabla_{ij}^2 \\ L_{ij}^{21}(\vec{r})\nabla_{ij}^2 & L_{ij}^{22}(\vec{r})\nabla_{ij}^2 & L_{ij}^{23}(\vec{r})\nabla_{ij}^2 & L_{ij}^{24}(\vec{r})\nabla_{ij}^2 \\ L_{ij}^{31}(\vec{r})\nabla_{ij}^2 & L_{ij}^{32}(\vec{r})\nabla_{ij}^2 & L_{ij}^{33}(\vec{r})\nabla_{ij}^2 & L_{ij}^{34}(\vec{r})\nabla_{ij}^2 \\ L_{ij}^{41}(\vec{r})\nabla_{ij}^2 & L_{ij}^{42}(\vec{r})\nabla_{ij}^2 & L_{ij}^{43}(\vec{r})\nabla_{ij}^2 & L_{ij}^{44}(\vec{r})\nabla_{ij}^2 \end{pmatrix} \end{array}, \tag{A.2}$$

where each of the matrix components $L_{ij}^{\alpha\beta}(\vec{r})$ for fixed $\alpha\beta$ forms a scalar product with the operator ∇_{ij}^2. The components $D_{ij}^{\alpha\beta}(\vec{r})$ and $L_{ij}^{\alpha\beta}(\vec{r})$ have very similar form. The deformation potential components $D_{ij}^{\alpha\beta}(\vec{r})$ are

$$D_{ij}^{11}(\vec{r}) = D_{ij}^{22}(\vec{r}) = \begin{bmatrix} a+\frac{b}{2} & 0 & 0 \\ 0 & a+\frac{b}{2} & 0 \\ 0 & 0 & a-b \end{bmatrix},$$

$$D_{ij}^{33}(\vec{r}) = D_{ij}^{44}(\vec{r}) = \begin{bmatrix} a-\frac{b}{2} & 0 & 0 \\ 0 & a-\frac{b}{2} & 0 \\ 0 & 0 & a+b \end{bmatrix},$$

$$D_{ij}^{13}(\vec{r}) = D_{ij}^{31^*}(\vec{r}) = -D_{ij}^{24^*}(\vec{r}) = -D_{ij}^{42}(\vec{r}) = \begin{bmatrix} 0 & 0 & -i\frac{d}{2} \\ 0 & 0 & -\frac{d}{2} \\ -i\frac{d}{2} & -\frac{d}{2} & 0 \end{bmatrix},$$

$$D_{ij}^{14}(\vec{r}) = D_{ij}^{23^*}(\vec{r}) = D_{ij}^{32}(\vec{r}) = D_{ij}^{41^*}(\vec{r}) = \begin{bmatrix} \frac{\sqrt{3}}{2}b & -i\frac{d}{2} & 0 \\ -i\frac{d}{2} & -\frac{\sqrt{3}}{2}b & 0 \\ 0 & 0 & 0 \end{bmatrix},$$

$$D_{ij}^{12}(\vec{r}) = D_{ij}^{21}(\vec{r}) = D_{ij}^{34}(\vec{r}) = D_{ij}^{43}(\vec{r}) = \begin{bmatrix} 0 & 0 & 0 \\ 0 & 0 & 0 \\ 0 & 0 & 0 \end{bmatrix}, \tag{A.3}$$

where a, b and d are material constants. The Hamiltonian components $L_{ij}^{\alpha\beta}(\vec{r})$ can be obtained by making the substitutions $(\hbar^2/2m_0)\gamma_1 \leftrightarrow a$, $(\hbar^2/m_0)\gamma_2 \leftrightarrow b$, $(\sqrt{3}\hbar^2/m_0)\gamma_3 \leftrightarrow d$ into the expressions for the components $D_{ij}^{\alpha\beta}(\vec{r})$, where γ_1, γ_2, γ_3 are the Luttinger–Kohn parameters. Values for the deformation potential constants and the Luttinger–Kohn parameters for Si and Ge are given in the table below, taken from experimental measurements. Values for alloys of Si and Ge are interpolated from values for the bulk materials by means of the linear rule of mixtures.

	a (eV)	b (eV)	d (eV)	γ_1	γ_2	γ_3
Si	2.1	−1.5	−3.4	4.29	0.34	1.45
Ge	2.0	−2.2	−4.4	13.4	4.24	5.59

For cases in which the heavy hole and light hole valence subbands are assumed to be decoupled, the Hamiltonian function is of the form

$$H(\vec{r}) = L_{ij}\nabla_{ij}^2, \tag{A.4}$$

where the components of the tensor L_{ij} contain the effective masses associated with the principle crystallographic directions, and are written for the heavy hole case as

$$L_{11} = \frac{\hbar^2}{2m_0}(\gamma_1+\gamma_2), \quad L_{22} = \frac{\hbar^2}{2m_0}(\gamma_1+\gamma_2), \quad L_{33} = \frac{\hbar^2}{2m_0}(\gamma_1-2\gamma_2) \tag{A.5}$$

and for the light hole case as

$$L_{11} = \frac{\hbar^2}{2m_0}(\gamma_1-\gamma_2), \quad L_{22} = \frac{\hbar^2}{2m_0}(\gamma_1-\gamma_2), \quad L_{33} = \frac{\hbar^2}{2m_0}(\gamma_1+2\gamma_2). \tag{A.6}$$

References

ABAQUS Finite Element Program, Version 5.7, Hibbitt, Karlsson and Sorensen, Inc., Pawtucket, RI, USA.

Akyüz, C.D., Zaslavsky, A., Freund, L.B., Syphers, D.A., Sedgewick, T.O., 1998. Inhomogeneous strain in individual quantum dots probed by transport measurements. Applied Physics Letters 72, 1739.

Brinkmann, D., Fishman, G., Gourgon, C., Dang, L.S., Löffler, A., Mariette, H., 1996. Excitons in CdTe quantum wires with strain-induced lateral confinement. Physical Review B 54, 1872–1876.

Eaglesham, D.J., Cerullo, M., 1990. Dislocation-free Stranski-Krastanow growth of Ge on Si (1 0 0). Physical Review Letters 64, 1943.

Eshelby, J.D., 1957. The determination of the elastic field of an ellipsoidal inclusion, and related problems. Proceedings of the Royal Society of London A 241, 376–396.

Faux, D.A., Downes, J.R., O'Reilly, E.P., 1997. Analytic solutions for strain distributions in quantum-wire structures. Journal of Applied Physics 82, 3754–3762.

Floro, J.A., Chason, E., Twesten, R.D., Hwang, R.Q., Freund, L.B., 1997. SiGe coherent islanding and stress relaxation in the high mobility regime. Physical Review Letters 79, 3946–3949.

Grundmann, M., Stier, O., Bimberg, D., 1995. InAs/GaAs pyramidal quantum dots: strain distributions, optical phonons, and electronic structure. Physical Review B 52, 11969–11981.

Johnson, H.T., Freund, L.B., Akyüz, C.D., Zaslavsky, A., 1998. Finite element analysis of strain effects on electronic and transport properties in quantum dots and wires. Journal of Applied Physics 84, 3714–3725.

Leonard, D., Krishnamurthy, M., Reaves, C.M., Denbaars, S.P., Petroff, P.M., 1993. Direct formation of quantum-sized dots from uniform coherent islands of InGaAs on GaAs surfaces. Applied Physics Letters 63, 3203.

Pryor, C., 1998. Eight-band calculations of strained InAs/GaAs quantum dots compared with one-, four-, and six-band approximations. Physical Review B 57, 7190–7195.

Singh, J., 1993. Physics of semiconductors and their heterostructures. McGraw-Hill, New York.

Williamson, A.J., Zunger, A., Canning, A., 1998. Prediction of a strain-induced conduction-band minimum in embedded quantum dots. Physical Review B 57, R4253–R4256.

Yang, M., Sturm, J.C., Prevost, J., 1997. Calculation of band alignments and quantum confinement effects in zero- and one-dimensional pseudomorphic structures. Physical Review B 56, 1973–1980.

Zaslavsky, A., Milkove, K.R., Lee, Y.H., Ferland, B., Sedgewick, T.O., 1995. Strain relaxation in silicon–germanium microstructures observed by resonant tunneling spectroscopy. Applied Physics Letters 67, 3921.

Zunger, A., 1998. Electronic-structure theory of semiconductor quantum dots. MRS Bulletin 23, 35–42.